Geophysical Research Letters

RESEARCH LETTER
10.1029/2019GL084540

Wind-Driven Strain Extends Seasonal Stratification

Eugenio Ruiz-Castillo, Jonathan Sharples[1], and Jo Hopkins[2]

[1]Department of Earth, Ocean and Ecological Sciences, University of Liverpool, Liverpool, UK, [2]National Oceanography Centre, Liverpool, UK

Key Points:
- A cross-shelf salinity gradient combined with wind-driven transport generates salinity strain that maintains/extends seasonal stratification
- Extending/maintaining the stratified period has implications for the timing of the phytoplankton bloom and bottom water ventilation
- Models do not reproduce the observed cross-shelf salinity gradients and fail to simulate the timing and duration of phytoplankton blooms

Correspondence to:
E. Ruiz-Castillo,
eugenio.ruiz@liverpool.ac.uk

Citation:
Ruiz-Castillo, E., Sharples, J., & Hopkins, J. (2019). Wind-Driven Strain Extends Seasonal Stratification. *Geophysical Research Letters*, *46*, 13,244–13,252. https://doi.org/10.1029/2019GL084540

Received 13 JUL 2019
Accepted 8 NOV 2019
Accepted article online 15 NOV 2019
Published online 27 NOV 2019

Abstract The onset and breakdown of stratification are key physical drivers of phytoplankton growth in shelf seas and the open ocean. We show how in the Celtic Sea, where seasonality in stratification is generally viewed as controlled by heat input, a cross-shelf salinity gradient horizontally strained by the wind prolonged the stratified period by 5–6 days in autumn prior to full winter mixing, while in spring caused seasonal stratification to begin 7 days early. Salinity straining has important implications for setting light conditions during the start of the spring bloom and for the timing of bottom-water ventilation in winter. Analysis of winds around the time of likely onset of spring stratification between 1979 and 2016 showed that in 60% of the years' wind conditions were favorable for salinity straining. Accurate knowledge of the horizontal salinity field and wind stress are required to correctly determine the onset and breakdown of stratification.

1. Introduction

In temperate shelf seas and the open-ocean seasonal vertical stratification is typically thought to depend on a competition between the capacity of atmospheric heat input to overcome tidal and wind-driven mixing (Kara et al., 2003; Simpson, 1981). However, stratification may be controlled by salinity when temperature is vertically homogenous. For example, in the thermally mixed upper 100 m of the Equatorial Pacific, a zonal salinity gradient combined with vertical shear of an eastward jet can lead to restratification of the water column throughout the winter (Roemmich et al., 1994). In regions of freshwater influence, during periods of reduced tidal mixing, stratification is controlled by salinity (Sharples & Simpson, 1995; Simpson & Souza, 1995). An extreme example of the role played by salinity may be found in the Arctic, where a fresher surface mixed layer is isolated from deeper, warmer, and more saline water by a strong halocline (Shaw et al., 2009; Toole et al., 2010). The onset and maintenance of stratification are vital for biological processes such as phytoplankton blooms (Pingree et al., 1976 and 1977; Taylor & Ferrari, 2011; Chiswell et al., 2013; Sigler et al., 2014). The survival of larval fish and the secondary production of higher trophic levels can then depend on the timing of the local phytoplankton spring bloom (Cushing, 1990; Platt et al., 2003) and the duration of these relatively short bloom events (Townsend et al., 1994). A second seasonal bloom occurs in autumn. Heat loss and intensified winds deepen the pycnocline (Wihsgott et al., 2019) and resupply surface waters with nutrients from the bottom layer (Chiswell et al., 2013; Ruiz-Castillo et al., 2019) leading to an autumn bloom (Chiswell et al., 2013; Pingree et al., 1976; Wihsgott et al., 2019). This autumn mixing is also important for ventilating the deeper water that has been isolated from contact with the atmosphere by the summer stratification (e.g., Greenwood et al., 2010). Understanding the driving mechanisms controlling the evolution of stratification is essential to comprehending the biogeochemistry of shelf seas.

Our study area is the Celtic Sea, a temperate shelf sea on the northwest European shelf (Figure 1a). The canonical view is that seasonal stratification in the Celtic Sea is a response to a competition between surface heating and vertical mixing processes (tides, wind, and surface heat loss driving convective mixing). In spring a positive net heat flux leads to the onset of stratification (Pingree et al., 1976 and 1977; Sharples et al., 2006; Wihsgott et al., 2019) and triggers the spring bloom (Carr et al., 2019; Garcia-Martin et al., 2019; Pingree et al., 1977), which continues until nutrients are depleted in the euphotic layer (Pemberton et al., 2004; Poulton et al., 2019). Throughout summer heat input enhances stratification and later in autumn stratification weakens as heat loss and wind stress deepen the surface mixed layer until reaching a fully mixed water column in winter (Wihsgott et al., 2019).

The prevailing winds in the Celtic Sea are westerly (Pingree, 1980). During the fully mixed winter months there are strong cross-shelf horizontal temperature and salinity gradients. Colder and fresher water, due

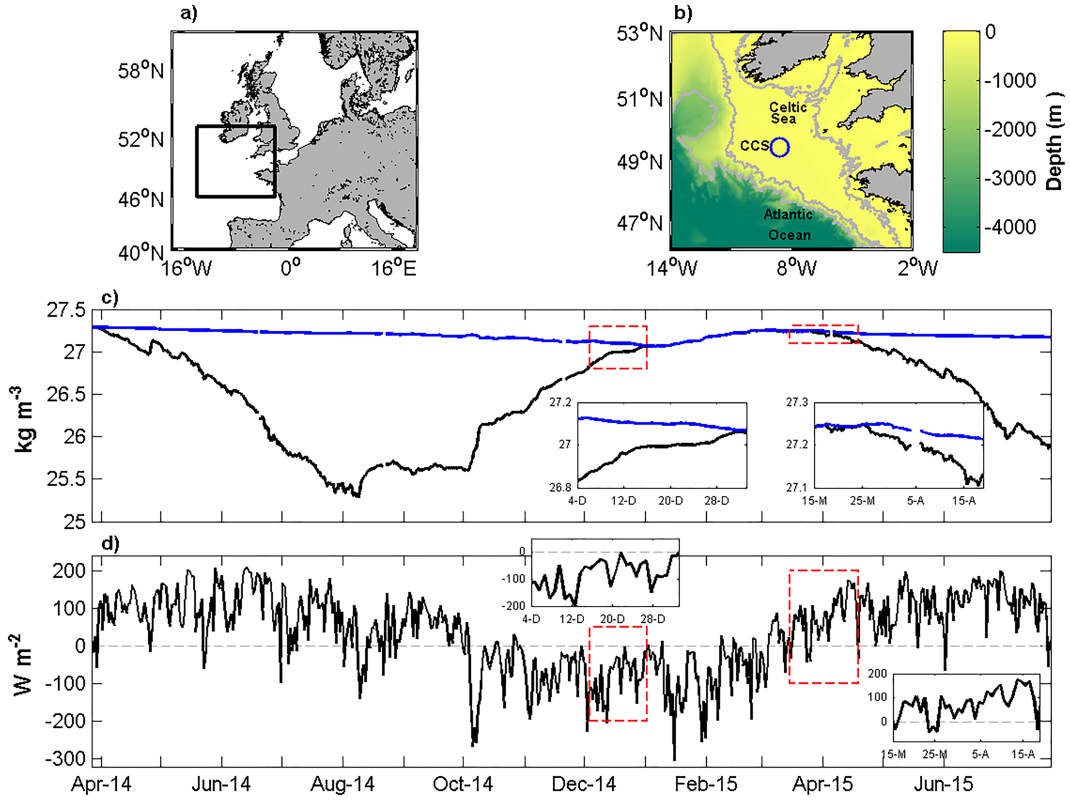

Figure 1. Map of the (a) north-western European shelf and (b) Celtic Sea. (c) Time series of surface (black) and bottom (blue) density and (d) net heat flux. The periods analyzed in this study are shown in the small boxes in (c) and (d).

to enhanced riverine discharge from the Bristol Channel (Brown et al., 2003; Ruiz-Castillo et al., 2019) combined with winter cooling of the relatively shallow water, is found near the coast, and warmer, saline water occupies the shelf edge. The Celtic Sea is therefore a transition zone between North Atlantic oceanic waters and fresher, estuarine origin waters (Brown et al., 2003; Ruiz-Castillo et al., 2019; Young et al., 2004). Near the coast, in the vicinity of the Bristol Channel, fresher waters may control up to 50% of the stratification in summer (Young et al., 2004). In the interior of the shelf it has been suggested that salinity may be important in controlling density in the early stages of the stratified period (Pingree et al., 1976; Horsburgh et al., 1998); however, the mechanisms that lead to this remain unclear. In this study we show that a simple view of seasonal surface atmospheric heat supply (or loss) and mixing does not always explain how seasonal stratification is triggered and maintained. We show how a cross-shelf salinity gradient horizontally strained by the wind is able to significantly extend the period of stratification by altering the timing of the onset and breakdown of stratification in spring and autumn.

2. Methods

2.1. Mooring Data

A 17-month (March 2014 to August 2015) full-depth time series of temperature and salinity from a mooring deployed at central Celtic Sea (CCS in Figure 1; 49.4°N, 8.6°W) (Wihsgott et al., 2016) was used to assess stratification of the 145-m-deep water column. Temporal resolution was 5 min, while vertical resolution ranged between 5 and 20 m in the surface and bottom layers and 2.5 m in the pycnocline region. Horizontal velocities between 20 m below the sea surface and 7 m above the seabed were recorded by a FlowQuest Acoustic Current Profiler, with a vertical bin size of 2 m and a temporal resolution of 2.5 min (see Wihsgott et al., 2018, for further details). There was an 8-day gap in the hydrographic and current measurements (4–12 April 2015) due to instruments being serviced during a research cruise (RRS *Discovery*, DY029). This gap was filled using 685 temperature and salinity profiles collected by a vertically profiling, wave-powered

Wirewalker (Pinkel et al., 2011) deployed between 5 and 11 April 2015, less than 1 km from the long-term mooring. An RBR-Concerto CTD recorded temperature and conductivity continually at 6 Hz and was calibrated against the ships' CTD (Hopkins et al., 2019). The 8-day servicing gap in the velocity record (4–12 April 2015) could not be filled. Temperature, salinity, and horizontal velocities were interpolated onto a regular grid with a temporal and spatial resolution of 5 min and 2.5 m, respectively. Conservative temperature, absolute salinity, and potential density were then calculated (McDougall & Barker, 2011). This work focuses on long-term fluctuations thus the semidiurnal signals associated with tidal currents were removed by using a low-pass Lanczos filter at each depth with a cut-off frequency of 24^{-1} h^{-1} (Thompson & Emery, 2014).

The vertical differences in conservative temperature, absolute salinity, and potential density between 35- and 105-m depths were calculated to assess density and thermal and haline stratification. Density at 35- and 105-m depths was also calculated using a fixed salinity (averaged salinity between 35 and 105 m) to estimate the contribution of thermal stratification to total stratification. Similarly, density was calculated using the averaged temperature between 35 and 105 m and used to quantify the contribution of haline stratification to total stratification. The depth-averaged (barotropic) component of flow was removed from the filtered velocities to obtain the velocity anomalies (u_c) at each time step.

2.2. Transport in the Surface and Bottom Layers

We calculate surface and bottom layer transport during the autumn (7 December 2014 to 1 January 2015) and spring (16 March to 20 April 2015) transition periods (red boxes in Figures 1c and 1d). In autumn 2014, the thickness of the surface (70–80 m) and bottom (50–70 m) mixed layers were determined by a density increase of 0.016 $kg{\cdot}m^{-3}$ and a decrease of 0.02 $kg{\cdot}m^{-3}$ from the surface and bottom, respectively. These thresholds are similar to the values utilized in Wihsgott et al. (2019). Defining distinct surface and bottom mixed layers based on density thresholds during the winter to spring transition, within which a continuous transport time series could be calculated, was not possible. Initially, an 80-m surface mixed layer was established. We therefore assume an 80-m-thick surface mixed layer throughout the entire spring transition and take the bottom mixed layer to be the lower 65-m of the water column. Transports in the surface and bottom layers were estimated by vertically integrating the horizontal velocity anomalies (u_c) at each time step within each layer.

2.3. Ekman Transport

The zonal (U_w) and meridional (V_w) components of the wind-driven Ekman transport were calculated from in situ hourly wind data provided by a meteorological buoy at CCS. Frequencies higher than $1/24$ h^{-1} were removed from the wind velocity time series using a low-pass band Lanczos filter (Thompson & Emery, 2014). We focus on the north-south component of the Ekman transport (V_w) that is normal to the cross-shelf density gradient and driven by the east-west component of wind stress (τ_x).

$$-V_w = \frac{\tau_x}{f\rho_s} \tag{1}$$

and

$$\tau_x = \rho_a C_d W^2, \tag{2}$$

where W represents the zonal component of the wind velocity at 10 m above the sea surface and ρ_s and f represent the surface density and the Coriolis parameter, respectively. The air density (ρ_a) was assumed to be constant at 1.3 $kg{\cdot}m^{-3}$ and the drag coefficient (C_d) related to wind speed by $C_d = 1 \times 10^{-3}(0.63 + 0.066W)$, following Smith and Barke (1975). The theoretical Ekman transport and the observed transport in the surface and bottom layers were averaged every 24 h and compared through a Pearson correlation coefficient (r).

2.4. Net Heat Flux

Net heat flux (Q_T) was calculated using time series of meteorological data from the CCS site (Figure 1b) combined with shortwave radiation and total cloud cover from European Centre for Medium-Range Weather Forecasts Re-Analysis interim (ERA-interim) (Dee et al., 2011), a global atmospheric reanalysis product provided by the European Centre for Medium-Range Weather Forecasts in the form

$$Q_T = Q_S - (Q_B + Q_L + Q_C), \quad (3)$$

where Q_S, Q_B, Q_L, and Q_C represent incoming shortwave radiation, back radiation from the sea surface, and latent heat and sensible heat fluxes, respectively. Each component was estimated from bulk formulae following Gill (1982) (see also Holt & James, 1999).

3. Results

3.1. Late Autumn 2014

The ocean started losing heat to the atmosphere in October 2014 (Figure 1d) and the density difference between surface and bottom waters decreased throughout October, November, and December (Figure 1c). The water column became fully mixed on 1 January 2015. Through the preceding month, there was a 21-day period (7–28 December 2014) of sustained westerly winds, averaging 7.2 $m \cdot s^{-1}$ (Figure 2a). During this time there was an observed off-shelf (southward) transport in the surface layer (Figure 2b, blue line) of up to 1.2 $m^2 \cdot s^{-1}$ and an onshore (northward) flow in the bottom layer (Figure 2b, black line). The estimated wind-driven Ekman transport (Figure 2b, red line) is strongly correlated with observed transport in the surface ($r = 0.79$) and bottom ($r = -0.79$) layers. These correlations are significant at the $p < 0.01$ level and provide evidence for southward wind-driven transport at the surface and a compensatory northward flow in the lower half of the water column.

Decreases in salinity at CCS were consistent with wind-driven off-shelf transport in the surface layer bringing fresher water from the north toward the center of the shelf (Figure 2c). From 6 December the surface salinity, in a ~70-m-thick layer, gradually decreased from 35.61 $g \cdot kg^{-1}$ to minimum values of <35.55 $g \cdot kg^{-1}$ from 19 December onward. During this period the ERA-interim data indicated that <0.02 m of freshwater fell as rainfall at CCS, accounting for no more than 16% of the salinity decrease. This suggests that the wind-driven southward transport was the primary driver of the reduction in surface salinity. In the bottom layer relatively high salinities (>35.6 $g \cdot kg^{-1}$) were observed between 4 and 25 December, indicative of shelf-edge origin water being transported northward as a result of the wind-driven compensatory flow.

From 25 December onward the bottom water salinities began to decrease (Figure 2c). Between 25 and 31 December, water with salinities between 35.55 and 35.6 $g \cdot kg^{-1}$, previously observed at the surface between 7 and 19 December, reappeared at the bottom (Figure 2c). Southward wind-driven transport ensured fresher waters from north of the CCS occurred above the pycnocline and a stable vertical salinity gradient was maintained. There was >1 °C decrease in surface temperature, from over 12 °C on 4 December to less than 11 °C on 1 January 2015 (Figure 2d), consistent with a net loss of heat to the atmosphere (Figure 1d). The bottom water remained colder than the surface water until 28 December. Between 28 December and 1 January bottom water temperatures were greater than those at the surface, but the water column was stably stratified as a result of salinity strain (Figure 2e), with fresher waters, advected by the wind from the north of CCS, occurring in the surface layer.

Density stratification was mainly controlled by temperature between 7 and 11 December (Figure 3a) and until 15 December vertical differences in temperature controlled more than 50% of the density stratification (Figure 3b). After 15 December the vertical difference in salinity controlled more than 50% of the water column stratification, maintaining a stable vertical density gradient for 16 days until 1 January 2015. The role played by salinity in delaying the breakdown of stratification is demonstrated by considering the potential energy anomaly (PEA), a measure of work required to bring about complete vertical mixing of a stratified water column (Simpson, 1981; Simpson & Sharples, 2012). On 7 December the PEA was 50 $J \cdot m^{-3}$. Considering heat loss to the atmosphere and tidal and wind mixing from 7 December onward, the PEA would be expected to decrease from 50 to 0 $J \cdot m^{-3}$ by 26 December. Thus, complete mixing of the water column would have occurred on 26 December if stratification had been controlled solely by temperature. Instead, wind-driven salinity strain prolonged the stratified period by 5–6 days until 1 January 2015.

3.2. Early Spring 2015

Westerly winds occurred for 10 days between 26 March and 4 April (Figure 2f), with a positive net heat flux beginning on 26 March (Figure 1d). Between 5 and 11 of April the winds were easterly. A second period of easterly winds started on 15 April. Prior to 5 April strong correlations were found between the Ekman

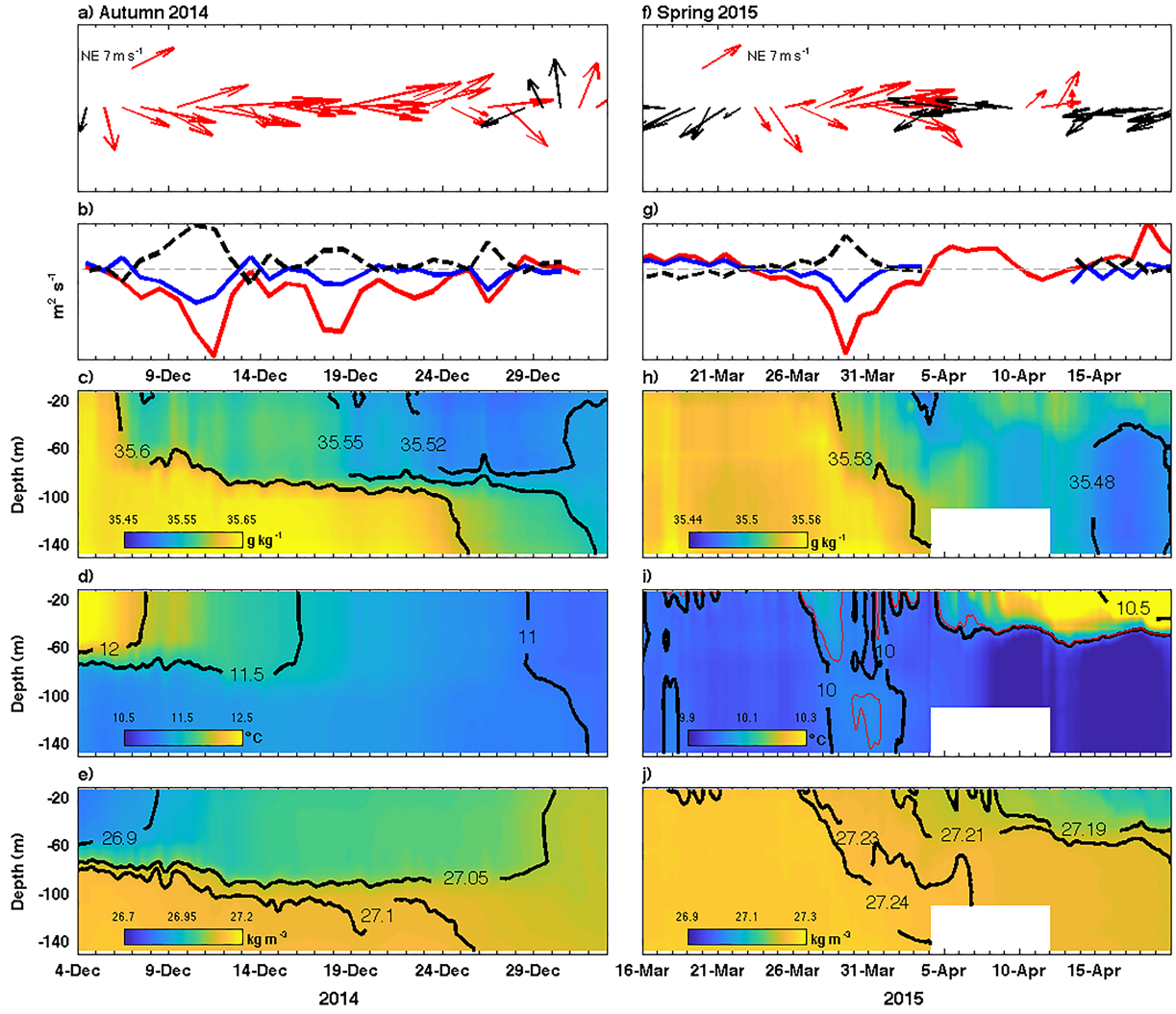

Figure 2. Time series for late autumn of (a) wind velocity, (b) transport in the surface (blue), and bottom (black) layers and the Ekman transport (red). Full-depth time series of (c) absolute salinity, (d) conservative temperature, and (e) potential density. (f–j) as in (a) to (e) but for early spring 2015. In (a) and (f) red (black) vectors indicate westerly (easterly) winds, and in (i) the red contour represents the 10.02 °C isotherm.

transport and the observed transport in the surface and bottom layers (r = 0.95 and −0.95, respectively), suggesting that the off-shelf surface transports and bottom on-shelf transports were wind driven (Figure 2g). Maximum southward (surface layer) and northward (bottom layer) transports (>1.3 $m^2 \cdot s^{-1}$) occurred between 26 March and 4 April (Figure 2g).

The water column was fully mixed between 16 and 26 March with a salinity >35.53 $g \cdot kg^{-1}$ and a temperature <10 °C (Figures 2h and 2i). There was a 0.05-$g \cdot kg^{-1}$ decrease in salinity over the top 80 m of the water column between 29 March and 4 April (Figure 2h) coincident with the maximum southward transport in the surface layer (Figure 2g). At the end of 28 March salinity in the upper 80 m was 35.536 $g \cdot kg^{-1}$. Between 29 March and 4 April there was <0.005 m of rainwater, which would have decreased the salinity by 0.002 to 35.534 $g \cdot kg^{-1}$. This small amount of freshening is <5% of the total decrease in salinity that was observed between 29 March and 4 April. We therefore attribute the reduction in salinity between the 29 March and 4 April to wind-driven transport of fresher waters (<35.53 $g \cdot kg^{-1}$) from the north of the Celtic Sea. After 4 April salinity increases in the surface layer were generated by easterly wind events in periods 4 and 11 April and 17 and 20 April.

A weak positive heat flux during daylight hours between 17 and 24 March drove warming (>10 °C) within the upper 25 m of the water column, with night time convection after each day (Figure 2i). Between 26 and

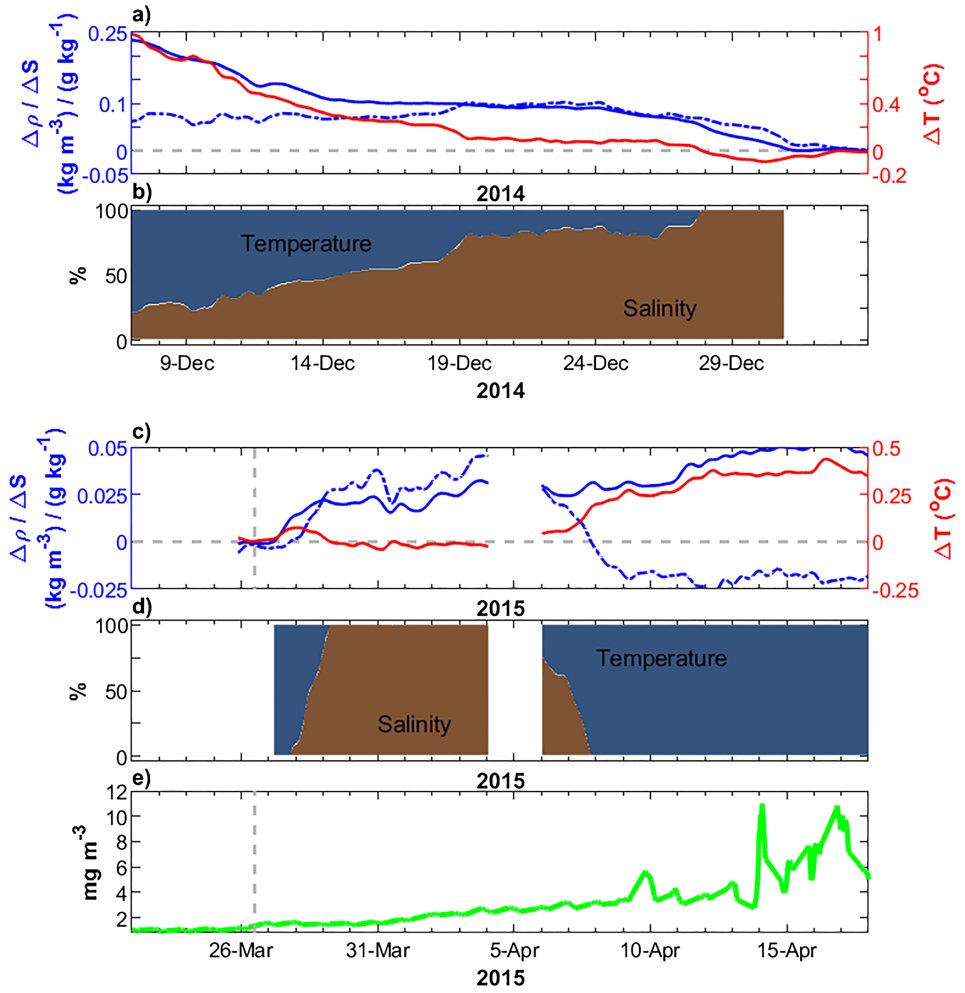

Figure 3. Vertical difference of conservative temperature (red), absolute salinity (dashed blue), and potential density (solid blue) between 35- and 105-m depths in (a) late autumn and (c) early spring. Percentage of stratification explained by vertical salinity (red) and temperature (blue) differences for (b) late autumn and (d) early spring. (f) Time series of surface Chl-*a* concentration. In (a) and (c), negative values indicate instability.

29 March the temperature within the upper 70–80 m increased and remained above 10 °C, coincident with a period of sustained positive net heat flux (Figure 1d). Subsequently from 29 March until 2 April the temperature decreased within the surface mixed layer (Figure 2i, red contour) despite a positive net heat flux (Figure 1d). At the same time the temperature of the bottom 50–60 m increased. The 10.02 °C isotherm is contoured in Figure 2i to help show this episode of surface layer cooling and bottom layer warming. Consequently, there were at least 5 days when the surface waters were colder than those at the bottom. This distribution of temperature was consistent with wind-driven advection of colder, lower salinity waters, from the northern Celtic Sea toward the shelf-edge at the surface and a return flow of slightly warmer, higher salinity waters of shelf-edge origin at the bottom.

From 6 April onward temperature gradually increased from 10 to >10.5 °C in the upper 30 m and remained higher than temperature in the bottom mixed layer (Figure 3c). From 7 April onward the vertical distribution of density resembled the temperature time series. Deepening of the 27.24 kg·m^{-3} contour indicates stratification at CCS started on 26 March (Figure 2j) consistent with the beginning of sustained positive net heat flux (Figure 1d). The vertical difference in temperature reached a maximum (~0.1 °C) on 28 March and gradually decreased until being unstable between 29 March and 4 April (Figure 3c). In contrast, stratification due to salinity gradually increased from 28 March until 4 April when the maximum difference was observed (0.05 g·kg^{-1}). Between 28 March and 7 April the vertical differences in salinity controlled between 50% and

100% of the water column stability (Figure 3d). From 5 April onward the vertical differences in salinity started to decrease. On 8 April salinity stratification became unstable and positive thermal stratification started to intensify and by 8 April temperature was 100% in control of water column stratification (Figure 3d). The vertical difference in salinity controlled 50% or more of the stratification for 10 days (29 March and 7 April).

Considering only heat input and tidal and wind mixing, the PEA would have increased from 0 on 25 March to 1.4 $J{\cdot}m^{-3}$ on 28 March. However, on 29 March energy input from the wind and tide would have fully remixed the water column (returning PEA to 0 $J{\cdot}m^{-3}$). Based only on heat flux, it would not have restratified again until 1 April. Instead, despite colder waters in the surface layer, wind-driven salinity straining maintained the stratification and increased the PEA to >4 $J{\cdot}m^{-3}$ by the 1 April.

4. Discussion

A cross-shelf salinity gradient in the Celtic Sea combined with wind-driven transport prolonged the stratified period in autumn and made sustained stratification occur earlier in spring. During late-autumn 2014 salinity controlled between 50% and 100% of water column stability prolonging the stratified period for 5–6 days prior to winter mixing. In the period 29 March to 7 April salinity controlled more than 50% of the water column stratification (Figure 3d), despite a relative cooling of surface water, and resulted in seasonal stratification being maintained 7 days early compared to expectations based on net heat flux.

Altering the timing of the onset and breakdown of seasonal stratification has implications for the biogeochemistry of the water column. In late autumn, extending the stratified period may not generate significant additional phytoplankton growth in the autumn bloom, as by mid-October light has become a limiting factor (Wihsgott et al., 2019). However, delays in autumn remixing will affect the timing of the ventilation of the bottom mixed layer, that is, reoxygenation of bottom waters, which have been isolated from the atmosphere through summer (Chen et al., 2007; Greenwood et al., 2010) and CO_2 exchange with the atmosphere as a result of relatively high dissolved inorganic carbon increasing in bottom waters through summer (Chen, 2010; Liu et al., 2010).

In spring, when nutrients are not limiting, earlier sustained stability of the water column increases the light available to phytoplankton in the surface mixed layer sooner, which results in an earlier spring bloom. This may have important implications for the succession of biological events that follow, for example, the survival of larval fish and secondary production of higher trophic levels (Cushing, 1990; Platt et al., 2003). At CCS surface chlorophyll-*a* concentrations (chlorophyll-*a* fluorescence) began increasing on 26 March 2015 (Figure 3e) as soon as thermal stratification started (Figures 2j and 3d). Chlorophyll-*a* fluorescence continued to increase through the time when salinity governed stability of the water column. Chlorophyll-*a* peaks were subsequently observed on 14 and 17 April. As a result of the salinity stratification the spring bloom developed over a period of ~20 days. This is twice the time that the bloom developed over in 2014 (Wihsgott et al., 2019). The development of spring stratification in 2014 was wholly driven by surface heat flux, quickly leading to a shallow, strongly stratified surface layer. The peak chlorophyll concentration seen in the 2014 bloom was about 5 $mg{\cdot}m^{-3}$ (Wihsgott et al., 2019) compared to 10 $mg{\cdot}m^{-3}$ in 2015 (Figure 3e), despite an initially slightly lower concentration of available nutrients (nitrite + nitrate) (7 $mmol{\cdot}m^{-3}$ in 2015 compared to 8 $mmol{\cdot}m^{-3}$ in 2014 of $NO_2 + NO_3$; Ruiz-Castillo et al., 2019). Thus, as well as an earlier start to sustained phytoplankton growth, the greater time over which the bloom occurred could result in overall greater production during the spring bloom. The period of initially weak and relatively deep stratification potentially allowing more nutrients to be available in the surface layer (30 m × 8 $mmol{\cdot}m^{-3}$ = 240 $mmol{\cdot}m^{-2}$ in 2014 compared to 80 m × 7 $mmol{\cdot}m^{-3}$ = 560 $mmol{\cdot}m^{-2}$ in spring 2015) and delaying the usual drawdown of surface layer nutrients in response to phytoplankton uptake.

Finally, we can estimate how often the spring bloom might be affected by horizontal straining. In the Celtic Sea the spring stratified period typically begins between March and April (Fasham et al., 1983). Westerly winds are most prevalent (Pingree, 1980) and are favorable for off-shelf advection of cold and fresher waters in the surface layer from the north of the shelf. Using ERA-interim data sets (Dee et al., 2011) we have estimated the percentage of years that westerly winds coincide with the expected beginning of stratification. If the onset of stratification takes place between 15 March and 15 April, 60% of the years between 1979 and

2016 had winds in this period that were favorable for straining of the horizontal salinity field and associated development of stratification. Thus, overall salinity strain is potentially more important than heat input in controlling the onset of sustained stratification and the timing of the spring bloom in the Celtic Sea.

The magnitude of the earlier onset of spring stratification is similar to model estimates of the interannual variability in bloom timing on the NW European shelf when considering surface heating as the only source of buoyancy (Sharples et al., 2006). Regional models of the NW European shelf are often unable to reproduce observed cross-shelf salinity gradients (e.g.,Young et al., 2004 ; Young & Holt, 2007), attributed to uncertainties in boundary conditions. If the wind-driven salinity straining is an important contributor to the control of the onset and breakdown of stratification, as we have observed here, then it is essential that modeled salinity fields are improved.

Acknowledgments
Eugenio Ruiz-Castillo was supported by a scholarship from The National Council for Science and Technology (CONACyT). Sharples and Hopkins were funded by the U.K. NERC–Defra Shelf Sea Biogeochemistry Programme (Grants NE/K002007/1, NE/K001701/1). All data sets for this research are freely available from the British Oceanographic Data Centre (http://www.bodc.ac.uk). Time series from moorings can be found in Wihsgott et al. (2016) and Wihsgott et al. (2018), and hydrographic profiles can be found in Hopkins et al. (2019).

References

Brown, J., Carrillo, L., Fernand, L., Horsburgh, K. J., Hill, A. E., Young, E. F., & Medler, K. J. (2003). Observations of the physical structure and seasonal jet-like circulation of the Celtic Sea and St. Georges Channel of the Irish Sea. *Continental Shelf Research*, *23*(6), 533–561. https://doi.org/10.1016/S0278-4343(03)00008-6

Carr, N., Davis, C., Blackbird, S., Daniels, L. R., Preece, C., Woodward, M., & Mahaffey, C. (2019). Seasonal and spatial variability in the optical characteristics of DOM in a temperate shelf sea. *Progress in Oceanography*, *177*, 101929. https://doi.org/10.1016/j.pocean.2018.02.025

Chen, C.-C., Gong, G.-C., & Shiah, F.-K. (2007). Hypoxia in the East China Sea: One of the largest coastal low-oxygen areas in the world. *Marine Environmental Research*, *64*(4), 399–408. https://doi.org/10.1016/j.marenvres.2007.01.007

Chen, C.-T. A. (2010). Ch. 3, Cross-boundary exchanges of carbon and nitrogen in continental margins. In K.-K. Liu, L. Atkinson, R. Quiones, & L. Talaue-McManus (Eds.), *Carbon and nutrient fluxes in continental margins*, *Global Change—The IGBP Series*, (pp. 53–97). Berlin, Heidelberg: Springer.

Chiswell, S. M., Bradford-Grieve, J., Hadfield, M. G., & Kennan, S. C. (2013). Climatology of surface chlorophyll a, autumn-winter and spring bloom in the southwest Pacific Ocean. *Journal of Geophysical Research: Oceans*, *118*, 1003–1018. https://doi.org/10.1002/jgrc.20088

Cushing, D. H. (1990). Plankton production and year-class strength in fish populations: An update of the match/mismatch hypothesis. *Advances in Marine Biology*, *26*, 249–294. https://doi.org/10.1016/S0065-2881(08)60202-3

Dee, D. P., Uppala, S. M., Simmons, A. J., Berrisford, P., Poli, P., Kobayashi, S., et al. (2011). The ERA-Interim reanalysis: Configuration and performance of the data assimilation system. *Quarterly Journal of the Royal Meteorological Society*, *137*, 553–597. https://doi.org/10.1002/qj.828

Fasham, M. J. R., Holligan, P. M., & Pugh, P. R. (1983). The spatial and temporal development of the spring phytoplankton bloom in the Celtic Sea, April, 1979. *Progress in Oceanography*, *12*(1), 87–145. https://doi.org/10.1016/0079-6611(83)90007-1

Garcia-Martin, E. E., Daniels, C. J., Davidson, K., Lozano, J., Mayers, K. M. J., McNeill, S., et al. (2019). Plankton community respiration and bacterial metabolism in a North Atlantic Shelf Sea during spring bloom development (April 2015). *Progress in Oceanography*, *177*, 101873. https://doi.org/10.1016/j.pocean.2017.11.002

Gill, A. *Atmosphere-ocean dynamics. International Geophysics Series*, Vol. 30. New York: Academic Press. 1982.

Greenwood, N., Parker, E. R., & Fernand, L. (2010). Detection of low bottom water oxygen concentrations in the North Sea; implications for monitoring and assessment of ecosystem health. *Biogeosciences*, *7*(4), 1357–1373. https://doi.org/10.5194/bg-7-1357-2010

Holt, J., & James, I. D. (1999). A simulation of the southern North Sea in comparison with measurements from the North Sea Project Part 2 Suspended Particulate matter. *Continental Shelf Research*, *19*(12), 1617–1642. https://doi.org/10.1016/S0278-4343(99)00032-1

Hopkins, J., E. Jones, J. Kenny, C. A. Balfour. 2019. Temperature and salinity profiles from a vertically profiling float ("Wirewalker") deployed in the Celtic Sea during Uk Shelf Sea Biogeochemistry cruise RRS Discovery Dy029 in April 2015. British Oceanographic Data Centre, National Oceanography Centre, NERC.https://www.bodc.ac.uk/data/published_data_library/catalogue/10.5285/8f1ffe5a-3e34-2a60-e053-6c86abc08d3d/

Horsburgh, K., Hill, A. E., & Brown, J. (1998). A summer jet in the St. Georges Channel of the Irish Sea. *Estuarine, Coastal and Shelf Science*, *47*(3), 285–294. https://doi.org/10.1006/ecss.1998.0354

Kara, A. B., Rochford, P. A., & Hurlburt, H. E. (2003). Mixed layer depth variability over the global ocean. *Journal of Geophysical Research*, *108*(C3), 3079. https://doi.org/10.1029/2000JC000736

Liu, K. K., L. Atkinson, R. A. Quiones, L. Talaue-McManus. 2010. Ch. 1, Biogeochemistry of continental margins in a global context, in carbon and nutrient fluxes in continental margins. *A global Synthesis* (pp. 3–24). *The IGBP Series*, Berlin-Heidelberg: Springer.

McDougall, T.J. P.M. Barker. 2011: *Getting started with TEOS-10 and the Gibbs Seawater (GSW) Oceanographic Toolbox*, 28. SCOR/IAPSO 193 WG127, ISBN 978-0-646-55621-5.

Pemberton, K., Rees, A. P., Miller, P. I., Raine, R., & Joint, I. (2004). The influence of water body characteristics on phytoplankton diversity and production in the Celtic Sea. *Continental Shelf Research*, *24*(17), 2011–2028. https://doi.org/10.1016/j.csr.2004.07.003

Pingree, R. D. 1980. Ch. 13, Physical oceanography of the Celtic Sea and English channel. In The north-west European shelf seas: The sea bed and the sea in motion II. In F. T. Banner, M. B. Collins and K. S. Massie. *Physical and Chemical Oceanography, and Physical Resources*. Amsterdam, Oxford, New York: Elsevier *Oceanography Series*.

Pingree, R. D., Holligan, P. M., Mardell, G. T., & Head, R. N. (1976). The influence of physical stability on spring, summer and autumn phytoplankton blooms in the Celtic Sea. *Journal of the Marine Biological Association of the United Kingdom*, *56*(4), 845–873. https://doi.org/10.1017/S0025315400020919

Pingree, R. D., Maddock, L., & Butler, E. I. (1977). The influence of biological activity and physical stability in determining the chemical distributions of inorganic phosphate, silicate and nitrate. *Journal of the Marine Biological Association of the United Kingdom*, *57*(4), 1065–1073. https://doi.org/10.1017/S0025315400026138

Pinkel, R., Goldin, M. A., Smith, J. A., Sun, O. M., Aja, A. A., Bui, M. N., & Hughen, T. (2011). The Wirewalker: A vertically profiling instrument carrier powered by ocean waves. *Journal of Atmospheric and Oceanic Technology*, *28*(3), 426–435. https://doi.org/10.1175/2010JTECHO805.1

Platt, T., Fuentes-Yaco, C., & Frank, K. T. (2003). Spring algal bloom and larval fish survival. *Nature*, *423*(6938), 398–399. https://doi.org/10.1038/423398b

Poulton, A. J., Davis, C. E., Daniels, C. J., Mayers, K. M. J., Harris, C., Tarran, G. A., et al. (2019). Seasonal phosphorous and carbon dynamics in a temperate shelf sea (Celtic Sea). *Progress in Oceanography*, *177*, 101872. https://doi.org/10.1016/j.pocean.2017.11.001

Roemmich, D., Morris, M., Young, W. R., & Donguy, J. R. (1994). Fresh equatorial jets. *Journal of Physical Oceanography*, *24*(3), 540–558. https://doi.org/10.1175/1520-0485(1994)024<0540:FEJ>2.0.CO;2

Ruiz-Castillo, E., Sharples, J., Hopkins, J., & Woodward, M. (2019). Seasonality in the cross-shelf physical structure of a temperate shelf sea and the implications for nitrate supply. *Progress in Oceanography*, *177*, 101985. https://doi.org/10.1016/j.pocean.2018.07.006

Sharples, J., Ross, O. N., Scott, B. E., Greenstreet, S. P. R., & Fraser, H. (2006). Inter-annual variability in the timing of stratification and the spring bloom in the north-western North Sea. *Continental Shelf Research*, *26*(6), 733–751. https://doi.org/10.1016/j.csr.2006.01.011

Sharples, J., & Simpson, J. H. (1995). Semi-diurnal and longer period stability cycles in the Liverpool Bay R. O. F. I. *Continental Shelf Research*, *15*(2-3), 295–313. https://doi.org/10.1016/0278-4343(94)E0003-5

Shaw, W. J., Stanton, T. P., McPhee, M. G., Morison, J. H., & Martinson, D. G. (2009). Role of the upper ocean in the energy budget of Arctic Sea ice during SHEBA. *Journal of Geophysical Research*, *114*, C06012. https://doi.org/10.1029/2008JC004991

Sigler, M. F., Stabeno, P. J., Eisner, L. B., & Napp, J. M. (2014). Spring and fall phytoplanktom blooms in a productive subarctic ecosystem, the eastern Bering Sea, during 1995-2011. *Deep-Sea Research Part II*, *109*, 71–83. https://doi.org/10.1016/j.dsr2.2013.12.007

Simpson, J., & Sharples, J. (2012). *Introduction to the physical and biological oceanography of shelf seas*, (p. 424). Cambridge: Cambridge University Press.

Simpson, J. H. (1981). The shelf-sea fronts: Implications of their existence and behaviour. *Philosophical Transactions of the Royal Society London A*, *302*(1472), 531–546. https://doi.org/10.1098/rsta.1981.0181

Simpson, J. H., & Souza, A. (1995). Semidiurnal switching of stratification in the region of freshwater influence of the Rhine. *Journal of Geophysical Research*, *100*(C4), 7037–7044. https://doi.org/10.1029/95JC00067

Smith, S. D., Banke, E. G. (1975). Variation of the sea surface drag coefficient with wind speed. *Royal Meteorological Society*. *101* (429), 665–673.

Taylor, J. R., & Ferrari, R. (2011). Shutdown of turbulent convection as a new criterion for the onset of spring phytoplankton blooms. *Limnology and Oceanography*, *56*(6), 2293–2307. https://doi.org/10.4319/lo.2011.56.6.2293

Thompson, R., & Emery, W. (2014). *Data analysis methods in physical oceanography*, (3rd ed.p. 701). Amsterdam: Elsevier.

Toole, J. M., Timmermans, M.-L., Perovich, D. K., Krishfield, R. A., Proshutinsky, A., & Richter-Menge, J. A. (2010). Influences of the ocean surface mixed layer and thermohaline stratification on Arctic Sea ice in the central Canada Basin. *Journal of Geophysical Research*, *115*, C10018. https://doi.org/10.1029/2009JC005660

Townsend, D. W., Cammen, L. M., Holligan, P. M., Campbell, D. E., & Pettigrew, N. R. (1994). Causes and consequences of variability in the timing of spring phytoplankton blooms. *Deep Sea Research, Part I*, *41*(5-6), 747–765. https://doi.org/10.1016/0967-0637(94)90075-2

Wihsgott J., J. Hopkins, J. Sharples, C. A. Balfour, E. Jones. 2018. Long-term, full depth observations of horizontal velocities spanning 17 months, collected in a temperate shelf sea (Celtic Sea) on the NW European Shelf. British Oceanographic Data Centre, Natural Environment Research Council, UK. https://dx.doi.org/10.5285/631ddd2a-48df-143b-e053-6c86abc0d49f

Wihsgott J., J. Hopkins, J. Sharples, E. Jones, C. A. Balfour. 2016. Long-term mooring observations of full depth water column structure spanning 17 months, collected in a temperate shelf sea (Celtic Sea). British Oceanographic Data Centre, Natural Environment Research Council, UK. https://www.bodc.ac.uk/data/published_data_library/catalogue/10.5285/389fe406-ebd9-74f1e053-6c86abc032a4/

Wihsgott, J. U., Sharples, J., Hopkins, J. E., Malcolm, E., Woodward, S., Greenwood, N., et al. (2019). Observations of vertical mixing in autumn and its effect on the autumn phytoplankton bloom. *Progress in Oceanography*, *177*, 102059. https://doi.org/10.1016/j.pocean.2019.01.001

Young, E. F., Brown, J., Aldridge, J. N., Horsburgh, K. J., & Fernand, L. (2004). Development and application of a three-dimensional baroclinic model to the study of the seasonal circulation in the Celtic Sea. *Continental Shelf Research*, *24*(1), 13–36. https://doi.org/10.1016/j.csr.2003.09.003

Young, E. F., & Holt, J. T. (2007). Prediction and analysis of long-term variability of temperature and salinity in the Irish Sea. *Journal of Geophysical Research*, *112*, C01008. https://doi.org/10.1029/2005JC003386